Zeng et al., 2018, Iron fertilization of primary productivity by volcanic ash in the Late Cretaceous (Cenomanian) Western Interior Seaway: Geology, https://doi.org/10.1130/G45304.1.

# SUPPLEMENTAL DATA

## METHODS

For inductively coupled plasma mass spectrometry (ICPMS) analysis, samples of the core were collected by drilling ~1 $cm^2$ areas at 30-cm intervals, and homogeneously powdered for digestion. Approximately 80-90 mg of each sample were digested in heated savillex (Teflon) beakers using a combination of ultrapure hydrofluoric, perchloric, nitric, and hydrochloric acids, as well as hydrogen peroxide and aqua regia. Upon complete digestion, the samples were diluted in ultrapure 2% nitric acid, and trace metal concentrations were measured by conventional ICPMS analysis.

Calibration of XRF measurements is challenging because of intrinsic lamination-scale (1-10 mm) heterogeneity in rocks, which is detectable by XRF core scanning but not by ICPMS analysis. Sampled ICPMS measurements were therefore used to calibrate more densely spaced XRF measurements by correlating averages of the five XRF intensities collected ≤ 1 cm from the center of each ICPMS sample. XRF measurements were first background subtracted by comparison to neighboring spectral regions free of fluorescence lines. Results for regressions of 141 data points indicate that elemental X-ray fluorescence was well correlated with concentration despite sample heterogeneity and matrix variations associated with lithologies ranging from marls to bentonites. The $R^2$ values of regression of fluorescence intensity against concentration of Al, Ti, Fe, Mo, and Cr, are 0.51, 0.39, 0.37, 0.62, and 0.31, respectively.

Microfossils were identified via thin section microscopy and classified into functional groups (biserial planktonic, planispiral and trochospiral planktonic, keeled planktonic, and benthic foraminifera) related to depth assemblages established by Leckie

(1987). Functional groups are defined by morphology, inferred growth rate, and relative water depth. Raw abundance and percent abundance of microfossil assemblages was performed by counting > 300 specimens (when possible) from thin section samples immediately below and above ash beds (11 sampled ash beds) (Supplemental Table DR1). Microfossils were counted by moving the thin section sample at 1 mm increments on a mechanical stage until the entire sample had been surveyed. At each count location, specimens were counted if they landed on or very near the horizontal reticule of the eyepiece and if their morphologies were distinguishable in the plane of the thin section. Specimens discounted from the total measurement included macrofossils (bivalves, ammonites, sponge spicules), microfossils whose morphologies were uncertain due to very poor preservation, foraminifera with fewer than four chambers preserved, and juvenile foraminifera with very small test size.

**Supplemental Table DR1. Raw Abundance and Percent Abundance of Representative Foraminiferal Morphotypes in Below and Above Ash Assemblages.**

| Ash Bed | Below Ash Bed | | | | Above Ash Bed | | | |
|---|---|---|---|---|---|---|---|---|
| | Biserial | Trochospiral + Planispial | Keeled | Benthic | Biserial | Trochospiral + Planispiral | Keeled | Benthic |
| 1 | 346 (38.40%) | 550 (61.04%) | 0 (0%) | 5 (0.55%) | 311 (51.75%) | 290 (48.25%) | 0 (0%) | 0 (0%) |
| 2 | 236 (26.11%) | 665 (73.56%) | 1 (0.11%) | 2 (0.22%) | 7 (1.49%) | 462 (98.51%) | 0 (0%) | 0 (0%) |
| 3 | 163 (23.87%) | 519 (75.99%) | 1 (0.15%) | 0 (0%) | 250 (41.53%) | 351 (58.31%) | 1 (0.17%) | 0 (0%) |
| 4 | 163 (23.87%) | 519 (75.99%) | 1 (0.15%) | 0 (0%) | 149 (24.75%) | 452 (75.08%) | 0 (0%) | 1 (0.17%) |
| 5 | 211 (23.71%) | 674 (75.73%) | 5 (0.56%) | 0 (0%) | 21 (4.29%) | 468 (95.71%) | 0 (0%) | 0 (0%) |
| 6 | 292 (32.41%) | 608 (67.48%) | 1 (0.11%) | 0 (0%) | 153 (27.32%) | 407 (72.68%) | 0 (0%) | 0 (0%) |
| 7 | 345 (38.50%) | 544 (60.71%) | 3 (0.33%) | 4 (0.45%) | 229 (39.62%) | 348 (60.21%) | 1 (0.17%) | 0 (0%) |
| 8 | 235 (30.92%) | 521 (68.55%) | 4 (0.53%) | 0 (0%) | 80 (21.56%) | 290 (78.17%) | 1 (0.27%) | 0 (0%) |
| 9 | 274 (37.59%) | 451 (61.87%) | 1 (0.14%) | 3 (0.41%) | 101 (23.93%) | 321 (76.07%) | 0 (0%) | 0 (0%) |
| 10 | 177 (29.69%) | 417 (69.97%) | 2 (0.34%) | 0 (0%) | 162 (39.80%) | 245 (60.19%) | 0 (0%) | 0 (0%) |
| 11 | 167(28.59%) | 417 (71.40%) | 0 (0%) | 0 (0%) | 150 (33.86%) | 291 (65.69%) | 1 (0.23%) | 1 (0.23%) |
| **Sum** | 2609 (30.59%) | 5885 (69.02%) | 19 (0.22%) | 14 (0.16%) | 1613 (29.09%) | 3925 (70.79%) | 4 (0.07%) | 2 (0.04%) |

**Supplemental Figure DR1. Photograph of selected core samples from Upper Eagle Ford Group marl (A), Lower Eagle Ford Group marl with ash layer (arrow) (B), and Buda Formation limestone (C). D-F: Pyrite and carbonaceous matter in ash layer from the Lower Eagle Ford Group. Ash layer contains opaque pyrite and carbonaceous matter (transmitted light) (D). Transmitted light (E) and reflected light (F) show that pyrite occurs within ash grains and around carbonaceous matter. These observations indicate that pyrite within ashes is authigenic, rather than a primary component of ashes**.

## REFERENCES

Leckie, R.M., 1987, Paleoecology of Mid-Cretaceous planktonic foraminifera: A comparison of open ocean and epicontinental sea assemblages: Micropaleontology, v. 33, p. 164-176, doi: 10.2307/1485491.

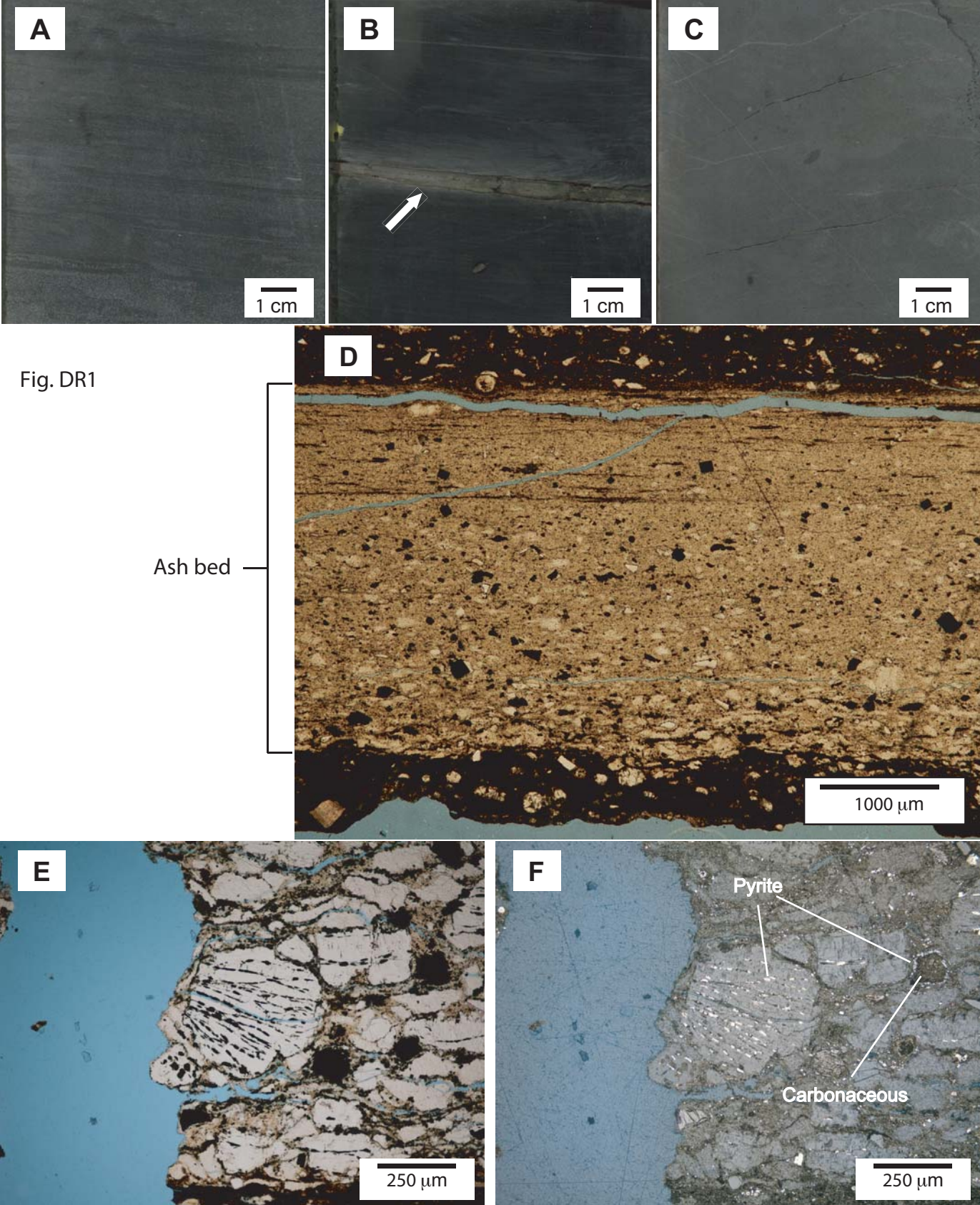
A
1 cm
B
1 cm
C
1 cm
D
Ash bed
1000 μm
E
250 μm
F
Pyrite
Carbonaceous
250 μm

Fig. DR1